Collision induced fragmentation of small ionic sodium clusters: Competition between electronic and impulsive mechanisms

M. Barat, J. C. Brenot, H. Dunet, J. A. Fayeton, and Y. J. Picard

Citation: J. Chem. Phys. **110**, 10758 (1999); doi: 10.1063/1.479019
View online: http://dx.doi.org/10.1063/1.479019
View Table of Contents: http://jcp.aip.org/resource/1/JCPSA6/v110/i22
Published by the AIP Publishing LLC.

Collision induced fragmentation of small ionic sodium clusters: Competition between electronic and impulsive mechanisms

M. Barat, J. C. Brenot, H. Dunet, J. A. Fayeton, and Y. J. Picard
Laboratoire des Collisions Atomiques et Moléculaires (UMR C8625), Université Paris-Sud, 91405 Orsay Cedex, France

(Received 3 February 1999; accepted 16 March 1999)

Collision induced fragmentation of small Na_n^+ $(n=3-9)$ clusters with He atoms is investigated in the 100 eV center-of-mass collision energy range. The experiment is based on the determination of the velocity vectors of the fragments using a multicoincidence technique. The relative populations of the various fragmentation pathways are determined. Fragmentation mechanisms are discussed in detail. The most important pathways are primarily populated via momentum transfer in elastic binary collisions between the He atom and a Na^+ core. Direct release of fast Na atoms is observed at variance with what is usually assumed at eV energies. However most of the fragmentation involves multistep dynamics with energy redistribution inside the cluster via Na–Na collisions. In contrast, production of Na^+ fragments comes dominantly from electronic transitions towards repulsive potential energy surfaces of the cluster. The role of electron pairing is emphasized. © *1999 American Institute of Physics.* [S0021-9606(99)01022-3]

I. INTRODUCTION

Collision induced dissociation (CID) of clusters attracted much interest both experimentally[1–12] and theoretically,[13–17] providing tools to study specific properties of clusters such as structures, dissociation pathways, and thermodynamical data. For example, measurements of total fragmentation cross sections at threshold[1–3] provide information on the bond energies. On the other hand, CID also offers a valuable tool to better understand the dynamics of ''finite'' size objects perturbed by heavy particle impacts. Indeed, the same basic mechanisms govern the CID of a molecule[18] or a cluster as well as the stopping power of an atomic particle in the bulk.[19] Such basic mechanisms are classified depending on the nature of the primary interaction. At high velocity (e.g., $\sim$1 a.u.) the perturbing particle primarily interacts with the electronic cloud. Considering for example interactions with a simple molecule, in a first step the molecule is brought up into an unbound excited state, then in a second step, the molecule dissociates, a mechanism referred to as *electronic* (EM). In contrast, at lower collision energy, typically below few keV, dissociation occurs if the atomic perturber transfers a large momentum in a close ''elastic'' collision with one atomic core of the molecule, a mechanism referred to as *impulsive* (IM). However, EM also operates at low energy. For example, when quasiresonant conditions are fulfilled, dissociative charge transfer dominates molecular dissociation processes.[20] In the medium-energy range where both EM and IM are simultaneously active, the dissociation mechanisms are considered as too complicated and, until recently not easily tractable by the available theoretical tools. At low eV collision energies, in the impulsive regime, a two step dissociation scenario is generally accepted.[4–7,13,14] In a first step, the perturber hits a unique atomic core of the cluster, the remainder of the cluster acting as a spectator. In a second step, the hit core transfers its momentum to the whole cluster through internal collisions. Hence heated, the cluster ''evaporates'' atomic fragments. In this ''spectator model'' the primary momentum transfer is generally treated with the impulsive model developed by Mahan[21] for translational to vibrational energy exchange in collinear collisions. For the second step, one generally assumes a statistical redistribution of the transferred energy within the cluster that is usually treated by the RRK theory.[22] Ejection of large fragments is sometimes explained assuming that initial electronic transitions are followed by direct fragmentation before randomization.[1,4] In this respect the various classes of clusters are expected to behave differently. Electronic transitions in metal clusters are expected to play an active role at variance with rare gas clusters as illustrated by the large electron capture cross sections in collisions between ionic alkali clusters and alkali atoms.[23]

To date, most of the experiments deal with measurements of total fragmentation cross sections using octupole-guiding structures to collect most of the fragments. Information on dissociation dynamics is then deduced from the energy dependence of cross sections for the various fragmentation channels.[1–7] Information is also provided by a measurement of the kinetic energy of the ionic fragment.[4] However, a detailed analysis of the kinematics of the fragmentation processes necessitates measurements of the momenta of all fragments.

We recently developed a new apparatus with a multicoincidence detection of charged and neutral particles allowing the simultaneous determination of the *velocity vectors* of all fragments produced in CID. The study of the CID of simple diatomic molecular ions such as Na_2^+,[24,25] K_2^+, and NaK^+ (Ref. 26) has been used as a test of this technique. The relative role of the electronic and impulsive mechanisms has clearly been identified. More complex processes involving initial momentum transfer in binary ''inelastic'' collisions

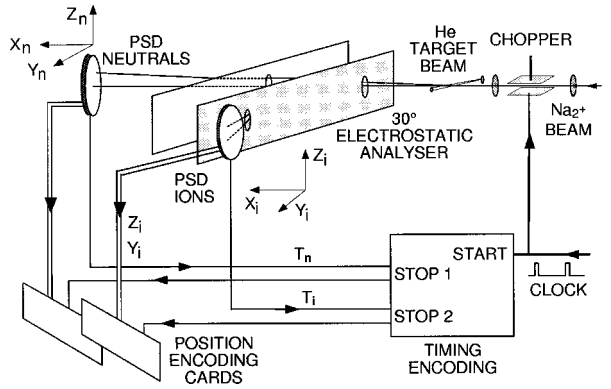

FIG. 1. Experimental setup.

have also been reported.[26] In the present paper we apply this technique to investigate fragmentation of small ionic sodium clusters ($Na_n^+ 2<n<10$) in collision with He at 60–200 eV center-of-mass (CM) collision energy.

II. EXPERIMENTAL TECHNIQUE (FIG. 1)

Only a brief description of the experimental setup is given here. A detailed account was presented in Ref. 25. The sodium clusters are produced in an expansion at the exit of an oven heated at 850 °C. They are ionized by 60 eV electrons, accelerated at 2 keV, and mass selected by a Wien filter. The cluster ion beam then crosses at 90° a ''cold'' He target beam produced by a supersonic expansion. The fragmented clusters then enter a parallel plate electrostatic analyzer. The neutral fragments fly in straight line through the analyzer and are received on a position sensitive detector (PSD). The ionic fragments are deflected in the electric field of the analyzer and detected on a second PSD in coincidence with the neutral fragments. The incident beam can be chopped at 1 MHz before collision. The chopper clock also triggers a multistop time-to-digital converter (TDC) that records the time of flight (TOF) of both the neutral and ionic fragments. The *velocity vectors* of the two fragments are determined from their locations on the two PSD and their TOF. For minor channels and largest clusters the very low intensity precludes from using the chopped beam technique. A factor 50–100 is gained in the beam intensity with the ''unchopped'' procedure. Information on kinematics is then obtained with an acceptable accuracy assuming a quasielastic collision. Comparing results obtained with and without chopping the beam provides confidence in this procedure. The collision volume and the analyzing device are biased with an additional voltage in order to get rid of the fragments produced by collision on the background gas or by evaporation of hot clusters along the incident trajectory. Because of their different energies, fragments produced in the collision volume are easily separated from the background fragments either by the electrostatic selector or/and by the TOF analysis. The cluster beam is initially accelerated at a constant voltage, but the bias voltage is adjusted in order to get the desired collision energy.

While the electrostatic analyzer can be tuned to select an ionized fragment of a given mass, the mass of the neutral fragments cannot be directly determined by the present technique. A ''fragmentation channel'' will then be identified by the mass of the detected ionic fragment. There is no ambiguity in the case of a $Na_{n-1}^+ + Na$ pathway. For others channels several neutral fragments can hit simultaneously the detector. The large dead-time for position encoding (3 μs) does not allow the simultaneous localization on the PSD of fragments coming from the same event. However, identification of such event is possible by measurements of the arrival times of all neutral fragments due to the much smaller dead-time of the time encoding (20 ns). The branching ratio P_{Na+Na/Na_2} between the $Na_{n-2}^+ + Na + Na$ and $Na_{n-2}^+ + Na_2$ pathways can then be estimated knowing the absolute detection efficiency (see Sec. III). A full analysis of the multifragmentation using a new detection device allowing simultaneous localization of two neutral fragments will be presented in a forthcoming paper.[27]

III. DETECTION EFFICIENCY

The knowledge of detection efficiencies for neutral and ionic fragments is necessary for determining fragmentation probabilities and branching ratio between different pathways. The present combination of heavy projectiles and light targets giving a nearly total collection of fragments (4π collection in the CM reference frame) allows determining the absolute detection efficiency of the MCP for Na atoms. Notice however that some neutral fragments can be scattered out of the PSD area for laboratory deflection angles larger than 3.2°. This limitation that does not significantly affect the determination of the detection efficiency, should be taken into account for data analysis. There is no such significant geometrical limitation for ionic fragments.

The method to determine the detection efficiency is based on the measurement of an ionic fragment in coincidence with a given neutral fragment by selecting the unambiguously identified $Na_n^+ \rightarrow Na_{n-1}^+ + Na$ channel. The ion and neutral counting rates, N_i and N_n measured on the two PSD are given by $N_i = \epsilon_i N_{tot}$ and $N_n = \epsilon_n N_{tot}$, respectively, where ϵ_i and ϵ_n stand for the ion and neutral detection efficiencies and N_{tot} is the total number of events. From the ion coincidence rate $N_{ic} = \epsilon_i \epsilon_n N_{tot}$, one easily gets $\epsilon_n = N_{ic}/N_i$. This method only allows determination of the detection efficiency for single atomic species and does not apply to ionic and neutral clusters since the corresponding fragmentation channels cannot be fully disentangled. The relationship between ϵ_n and kinetic energy for neutrals[28] compares well with that reported for various positive ions.[29] Hence we have assumed the same absolute efficiency for ionic and neutral clusters of the same energy. Notice that ϵ_n depends on the aging of the channel-plates. Therefore ϵ_n is remeasured before each set of experiments, a value used to determine the branching ratio,

$$P_{Na+Na/Na2} = \frac{2\frac{C_2}{C_1}}{\epsilon_n\left(1+2\frac{C_2}{C_1}\right)-2\frac{C_2}{C_1}}.$$

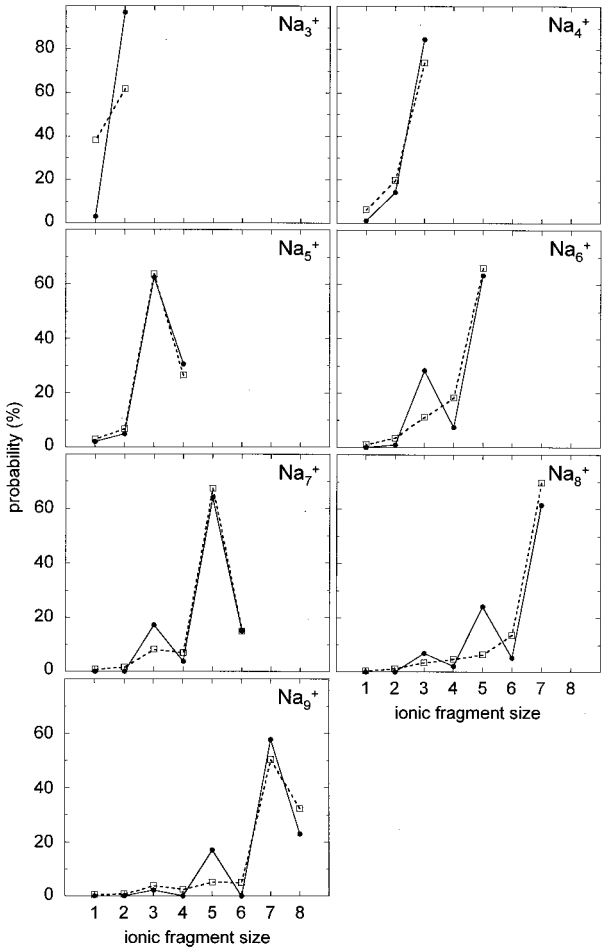

FIG. 2. Relative probabilities for the various fragmentation pathways identified by the ionic fragment at a same collision energy $E_{CM}=62$ eV. Full lines and closed dots: experimental data. Dashed lines and open squares, Estimates given by a simple model based on the endothermicities of the various channels (see text).

C_2 is the number of Na_{n-2}^+ ions detected in coincidence with two neutrals and C_1 is the number of Na_{n-2}^+ ions detected in coincidence with a unique neutral particle.

IV. FRAGMENTATION PROBABILITIES

The following method has been used to determine the relative fragmentation probabilities for the various pathways. The electrostatic selector is tuned to select an ionic fragment of a given size. In order to remove fluctuations in the projectile or target beams, the ionic counting rate is then normalized to the total neutral count rate received on the ''neutral'' PSD during the measurement time taking the ion detection efficiency into account. The results given in Fig. 2 for Na_3^+ to Na_9^+ cluster ions show the dominance of channels giving ionic fragments of the largest size with an even number of electrons.

V. THE ZZ CORRELATION

The correlation between locations on the vertical axis Z of the two detected fragments, abbreviated as the ''*ZZ* correlation'' gives a first insight into the fragmentation dynamics. The meaning of this correlation has been discussed in detail in Ref. 30 and is schematically recalled in Fig. 3. In brief, points localized inside the bottom-left and top-right squares, the slash structure, indicate a large deviation of the cluster center-of-mass (CCM) a signature of an *impulsive* character of the fragmentation process. On the other hand, points inside the other squares, the backslash structure, show dissociation without significant deviation of the CCM, a feature of the *electronic* mechanism. The slope of this structure is in inverse ratio of the mass fragments. In this respect, the two types of structures seen in the ''butterfly'' pattern for the Na_2^+ dimer fragmentation reflect the importance of both types of mechanisms.[24] A glance at Fig. 4 reveals two typical patterns:

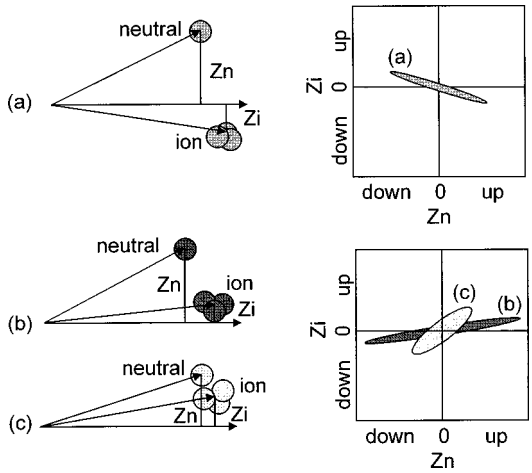

FIG. 3. Definition of the ZZ'' correlation (a) for *electronic* fragmentation, the deflection of the cluster CM is negligible; the neutral and the ionic fragments are ejected on opposite sides with respect to the incident beam direction. The vertical components of the fragment positions on the PSD Z_n and Z_i are, respectively, up and down for example and in the inverse ratio of the mass fragments. For a direct (b) or a two-step (c) *impulsive* fragmentation, the large deflection of the cluster CM results in ejection of fragments on the same side of the incident beam; Z_n and Z_i are both up or down.

(1) Channels giving Na^+ fragments show, at least for the smallest clusters, a rather vertical backslash, a clear indication of a dominance of the electronic mechanism.
(2) At variance for all other fragmentation channels, horizontal structures indicate a dominant impulsive character. Such patterns show *three* components: (i) a thin almost horizontal slash showing the ejection of a neutral fragment with a large velocity, (ii) a bulky pattern corresponding to fragments with small fragmentation velocities, and (iii) in some cases backslash structure characteristic of an electronic mechanism is superimposed to the bulky structure.

The $Na_n^+ \rightarrow Na_{n-1}^+ + Na$ channels located on the diagonal of Fig. 4 and corresponding to ejection of a *unique* Na atom are unambiguously identified. Therefore these pathways will be further analyzed in the next section while the ejection of a single Na^+ ion will be discussed in Sec. VII. Finally, specific comments will be addressed for the others pathways in Sec. VIII.

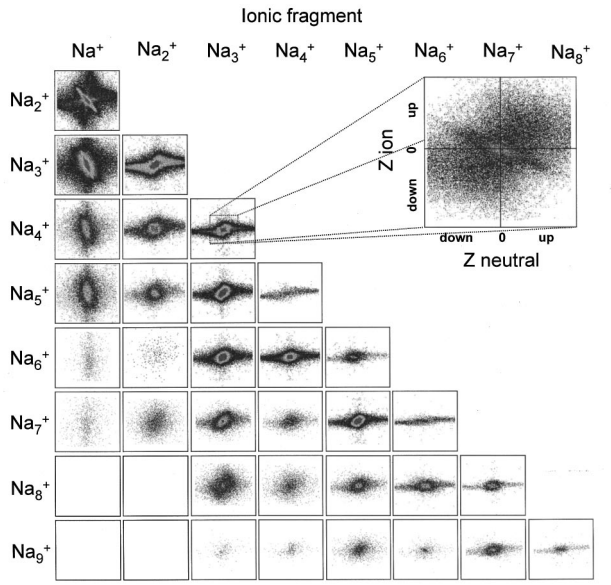

FIG. 4. ''*ZZ*'' correlation patterns, rows: Na_n^+ $(n=2-9)$ parent clusters, columns: identified ionic fragments. Insert: enlarged view of the ''bulky'' part of the $Na_4^+ \rightarrow Na_3^+ + Na$ pattern showing the two components corresponding to electronic and indirect impulsive mechanisms (IM2).

VI. THE $Na_{n-1}^+ + Na$ CHANNELS: BASIC FRAGMENTATION MECHANISMS

Appropriate parameters have to be chosen to well describe the collision process (Fig. 5). For example, the deflection angle χ of the CCM reflects the momentum transferred during the collision. The other parameters are $E_{\rm rel}$ the relative kinetic energy of the two fragments, α the orientation of the dissociation axis with respect to the scattered beam, and Φ the angle between the dissociation plane and the collision plane. Information on the energy loss ΔE that would nicely completes the description of the dynamics is not significant due to the energy spread of the incident beam. In particular such information should be necessary to fully identify transitions towards electronically excited states of the cluster. In any case the observables determined in the present experiment are relative values that are not significantly affected by the energy spread.

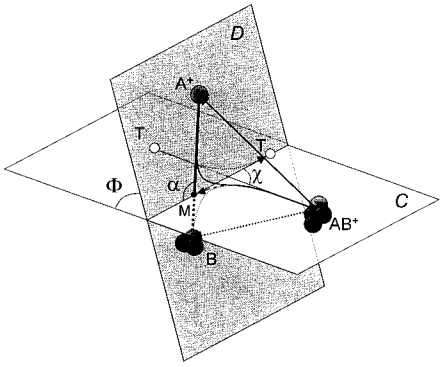

FIG. 5. Definition of the various collision parameters for $AB^+ + T \rightarrow A^+ + B + T$ fragmentation in the ABT center-of-mass frame χ: scattering angle of the cluster center of mass (M), Φ: angle between the collision plane (C) and the dissociation plane (D), α orientation of the AB^+ dissociation axis.

A. The slash structure in the ''*ZZ*'' correlation: Direct impulsive mechanism (IM1)

The simplest patterns appearing in Fig. 4 as a single horizontal line for Na_5^+ and Na_7^+ fragmentation is the signature of ejection of a fast Na fragment. The $E_{\rm rel}(\chi)$ correlation of Fig. 6(a) shows that the $Na_5^+ \rightarrow Na_4^+ + Na$ fragmentation begins at a threshold angle $\chi = 15°$. Then $E_{\rm rel}$ strongly increases with increasing χ. Let us consider a *one-step* impulsive mechanism, in which the Na^+ core hit by the He atom is directly ejected without significant interaction with the other Na^+ cores, a mechanism sometime called ''elastic'' collision.[13] For such direct impulsive mechanisms the $E_{\rm rel}(\chi) = (E_{\rm trans} - D)$ curves, where D is the endothermicity of the channel, can be estimated with a simple model[24] assuming a binary elastic collision between He and one Na^+ core at a χ_1 scattering angle. The energy transferred is given by

$$E_{\rm trans} = \frac{4(n-1)M_T(M_T + nM_{\rm Na})}{n^2(M_T + M_{\rm Na})^2} E_{\rm CM} \sin^2 \frac{\chi_1}{2}$$

with

$$\text{tg}\,\chi = \frac{\sin\chi_1}{\dfrac{(n-1)M_T}{nM_{\rm Na} + M_T} + \cos\chi_1} \quad \text{and} \quad E_{\rm CM} = \frac{M_T}{M_T + nM_{\rm Na}} E_0,$$

where M_T and $M_{\rm Na}$ are the target and the Na atom masses, respectively. E_0 is the laboratory collision energy. Since the internal energy $E_{\rm int}$ is unknown, the model curves are drawn for two limiting cases, $E_{\rm int} = 0$ and $E_{\rm int} = D$ corresponding to a hot cluster excited near the dissociation limit. The bond dissociation energies (endothermicity) of the various channels, reported in Table I,

$$D(Na_n^+ \rightarrow Na_{n-p}^+ + Na_p) = E_n^+ - E_{n-p}^+ - E_p$$

are determined from the absolute energies E_n^+ and E_n of the ionic and neutral clusters calculated by Lindsay *et al.*[31] However the experimental values of Bréchignac *et al.*[32] have been preferred for dimer and monomer evaporation energies.

It is readily seen in Fig. 6(a) that contour lines stretch, even for the largest energy transfers, along the curves given by this simple model. The $\Phi(\chi)$ correlation [Fig. 6(b)] shows that fragmentation takes place around the collision plane with the Na atom being side scattered $(\Phi = 0°)$ in agreement with the model as well as does the $\alpha(\chi)$ correlation [Fig. 6(c)]. Similar results are obtained for the release of a Na atom from a Na_7^+ cluster. It is noteworthy that such simple ''*ZZ*'' correlation patterns (Fig. 4) only appear in the two Na_5^+ and Na_7^+ cases for which the release of a single Na atom is not the less endothermic channel. Notice also that these channels are weakly populated (Fig. 2). Anticipating the discussion of Sec. VI B, this suggests that the additional mechanisms responsible for the bulky structure in the ''*ZZ*'' correlation of the $Na_n^+ \rightarrow Na_{n-1}^+ + Na$ pathway of even clusters $(n > 3)$ involve adiabatic relaxation towards the lowest

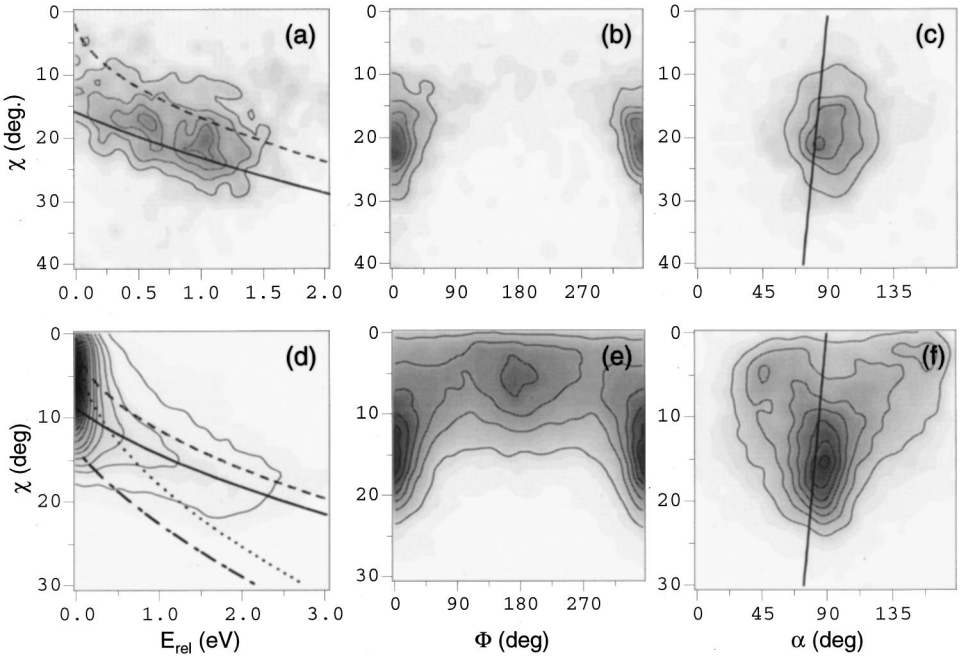

FIG. 6. $E_{rel}(\chi)$, $\Phi(\chi)$, and $\alpha(\chi)$ contour maps; (a) (b) (c) $Na_5^+ \rightarrow Na_4^+ + Na$ at $E_{CM}=87$ eV; (d) (e) (f) $Na_4^+ + Na_3^+ + Na$ at $E_{CM}=200$ eV. One-step impulsive model (IM1); full lines, the cluster is assumed to be in the vibrational ground state; dashed line, the cluster is vibrationally excited near the dissociation limit. Two-step impulsive model (IM2); dashed–dotted, the cluster is assumed to be in the vibrational ground state; dotted line, the cluster is vibrationally excited near the dissociation limit.

(ground state) fragmentation channel. In this respect, the next odd Na_9^+ cluster is a limit case for which the channels corresponding to the ejection of Na and Na_2 fragments[7] have very similar endothermicities. The weakness of the bulky structure observed in the *ZZ* correlation as well as the rather small population (Fig. 2) of the $Na_8^+ + Na$ channel are consistent with this analysis.

B. The bulky structure in the ''*ZZ*'' correlation: Electronic (EM) and two step impulsive (IM2) mechanisms

The $E_{rel}(\chi)$ diagram in Fig. 6(d) corresponds to the release of a single Na atom from Na_4^+ for which the double structure shows up in the ''*ZZ*'' correlation. The direct impulsive mechanism discussed above that is responsible for the linear structure in the ''*ZZ*'' correlation also appears in the $E_{rel}(\chi)$ diagram as contours which stretch along the curves of the IM model like in Fig. 6(a) for $Na_5^+ \rightarrow Na_4^+ + Na$. An enlargement of the central zone of the $Na_4^+ \rightarrow Na_3^+ + Na$ ''*ZZ*'' correlation is shown in the insert of Fig. 4. A close inspection reveals a backslash structure with a 1/3 slope, a clear signature of a fragmentation process induced by *electronic transitions* towards repulsive potential energy surfaces. This line is superimposed to a fuzzy cloud located in the ''impulsive region'' of the *ZZ* correlation (see Fig. 3). This structure reveals much smaller relative energies of the fragments and a more scattered distribution of the momenta. Comparing the $E_{rel}(\chi)$ diagram for $Na_5^+ \rightarrow Na_4^+$ and $Na_4^+ \rightarrow Na_3^+$ fragmentation [Figs. 6(a) and 6(d)], this bulky structure, referred to as IM2 clearly corresponds to contour lines stretching along the χ axis. The relative contributions of IM1, and IM2, and EM components in the $Na_4^+ \rightarrow Na_3^+$ pathway, are disentangled by first selecting the $E_{rel} < 0.3$ eV data that filters out the IM1 process. Then an adequate filtering of the two well-identified zones of the *ZZ* pattern separates the two remaining components finally leading to the

TABLE I. Relative contribution of the various mechanisms for the population of the $Na_n^+ \rightarrow Na_{n-1}^+$ and $Na_n^+ \rightarrow Na_{n-2}^+$ pathways. The sum of the contribution of all fragmentation pathways is normalized to 100. D(eV) is the corresponding endothermicity (see text). The laboratory collision energy is 5 keV except for Na_9^+ ($E_0=3.5$ keV). Mechanisms, IM2+EM means that it was not possible to disentangle the two contributions. (*) corresponds to an electronic transition with a simultaneous impulse transfer (Refs. 26 and 27).

Cluster	Pathway	Mechanism	Probability		D(eV)
		IM1	51		
	$Na_2^+ + Na$	IM2	31	92	1.38
Na_3^+		EM	9		
	$Na^+ + Na + Na$	EM	2.2	5.6	2.19
		*	3.4		
	$Na^+ + Na_2$	EM	2.4		1.43
		IM1	36		
	$Na_3^+ + Na$	IM2	24	80	0.58
Na_4^+		EM	20		
	$Na_2^+ + \underline{Na} + Na$	IM1	9.4		1.96
	$Na_2^+ + \overline{Na_2}$	EM	3.6		1.20
	$Na_4^+ + \underline{Na}$	IM1	30		0.87
Na_5^+	$Na_3^+ + \underline{Na} + Na$	IM1	24		1.50
	$Na_3^+ + \overline{Na_2}$	IM2	38		0.74
	$Na_5^+ + Na$	IM1	9	63	60
		IM2+EM	54		
Na_6^+	$Na_4^+ + \underline{Na} + Na$	IM1	4.8		1.68
	$Na_4^+ + \overline{Na_2}$	IM2<EM	2.6		0.92
	$Na_6^+ + \underline{Na}$	IM1	17		1.14
Na_7^+	$Na_5^+ + \underline{Na} + Na$	IM1	18		1.71
	$Na_5^+ + \overline{Na_2}$	IM2>EM	36		0.95
	$Na_7^+ + \underline{Na}$	IM1	6	61	0.76
		IM2+EM	55		
Na_8^+	$Na_6^+ + \underline{Na} + Na$	IM1	4.2		1.90
	$Na_6^+ + \overline{Na_2}$	IM2<EM	1		1.14
	$Na_8^+ + Na$	IM1	12	23	1.31
		IM2+EM	11		
Na_9^+	$Na_7^+ + \underline{Na} + Na$	IM1	22		2.07
	$Na_7^+ + \overline{Na_2}$	IM2+EM	35		1.31

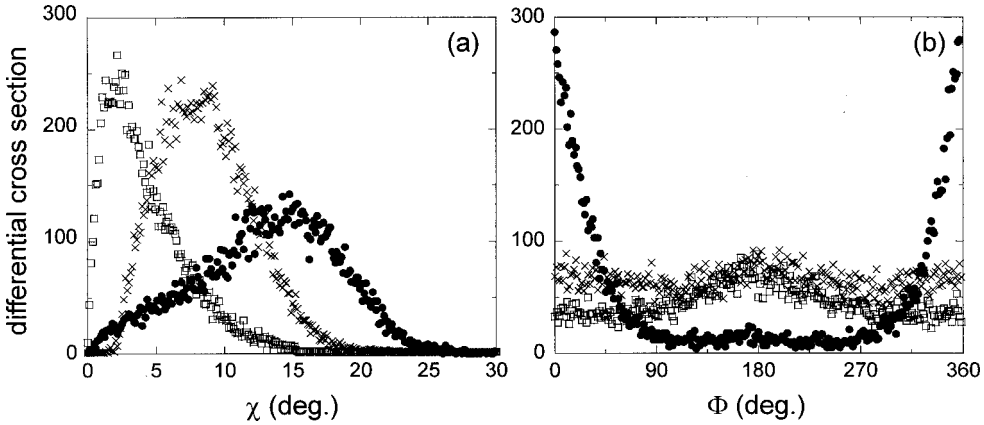

FIG. 7. Differential cross sections for the $Na_4^+ \rightarrow Na_3^+ + Na$ pathway, at $E_{CM} = 200$ eV (a) $I(\chi)$ and (b) $I(\Phi)$. Closed dots, IM1; crosses, IM2, open squares, EM contributions.

following contributions: IM1=45%, IM2=30%, and EM =25% at 200 eV CM energy. Differential cross sections (DCS) and Φ distributions for the three components hence disentangled are displayed in Figs. 7(a) and 7(b).

The component attributed to electronic fragmentation is peaked at the smallest angle, $\chi = 2°$ as expected when the transferred momentum is negligible. However, as a striking feature, the Φ distribution maximizes around 180° in contrast to that of the IM1 component. This feature also shows up as contours centered around $\chi = 5°$, $\Phi = 180°$ in the $\Phi(\chi)$ map [Fig. 6(e)]. At such χ, EM fragmentation is accompanied with additional momentum transfer[26] that forces the in-plane fragmentation. It is suggested that the preferential $\Phi = 180°$ peaking, corresponding to side scattered Na_{n-1}^+ fragments, is due to the probability for a He target to hit a Na^+ core that is roughly $(n-1)$ times larger in the large fragment.

The IM2 component shows a broad maximum around $\chi = 8°$ and is nearly *isotropically* distributed in Φ and α [Figs. 6(e), 6(f), and 7(b)]. The last of the initial collision plane suggests that IM2 fragmentation proceeds via a two-step mechanism. The momentum given during the initial Na^+–He hit, primarily characterized by the χ angle, is transferred in a second step to other Na^+ core(s) via Na–Na *intracluster* collisions. Such a two-step mechanism resulting in a sharing of the transferred energy among several Na atoms is nothing else but the mechanism generally invoked to explain fragmentation at eV collision energies.[4–7] For the largest clusters a statistical redistribution of the transferred energy to the various degrees of freedom can be assumed. The average kinetic energy release $\langle E_{rel} \rangle$ of the fragments can be estimated with a formula given by Engelking[33]

$$\langle E_{rel} \rangle = [E_{trans}(\chi) + E_{int} - D] \frac{2}{3n-7}.$$

The corresponding curves, drawn on the $E_{rel}(\chi)$ diagrams of Fig. 6(d) for Na_4^+ and Fig. 8 for Na_6^+ and Na_8^+ seem to account rather well for the stretching of the contour lines at small E_{rel} and large χ.

VII. CHANNELS PRODUCING Na^+ FRAGMENTS

The ejection of a single Na^+ ion, the most endothermic pathway is always the less populated channel (Fig. 2). The corresponding ''*ZZ*'' patterns are dominated by a nearly vertical linear structure characteristic of fragmentation induced by an electronic transition. The slope increasing with the size of the cluster is given by the mass ratio between the two fragments, a feature that points out the negligible momentum transfer. In addition to the dominant structure, the *ZZ* correlation shows additional fuzzy features appearing outside the main structure as particularly salient for the $Na_3^+ \rightarrow Na^+$ channel. They are interpreted as multifragmentation processes induced by electronic transitions with additional momentum transfer. The detailed analysis will be given elsewhere.[27]

VIII. OTHERS FRAGMENTATION CHANNELS

All other ''*ZZ*'' correlation patterns show a striking similarity with that discussed in Sec. VI calling for consideration of the same basic mechanisms. For example, the quasihorizontal slash of the ''*ZZ*'' correlation suggests again a fragmentation induced by a direct impulsive mechanism. However the lost of more than one Na atomic fragment can-

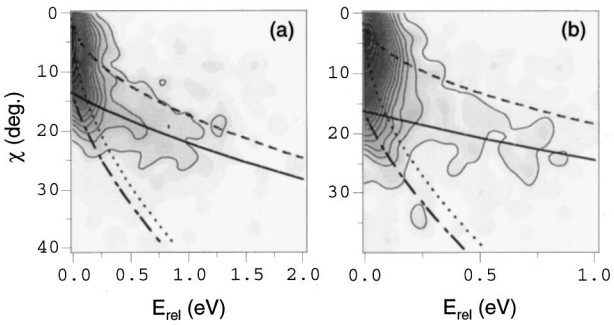

FIG. 8. $E_{rel}(\chi)$ contour maps. (a) $E_{rel}(\chi)$ for $Na_6^+ \rightarrow Na_5^+ + Na$ at $E_{CM} = 73$ eV; (b) $E_{rel}(\chi)$ for $Na_8^+ \rightarrow Na_7^+ + Na$ at $E_{CM} = 66$ eV. Prediction of the binary model as in Fig. 6.

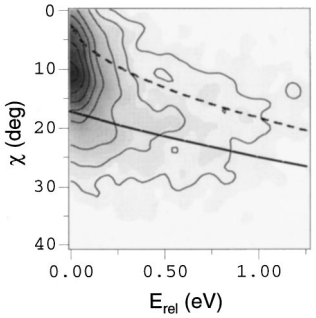

FIG. 9. $E_{\mathrm{rel}}(\chi)$ contour map for $Na_5^+ \rightarrow Na_3^+ + Na + Na$ fragmentation analyzed assuming a detection of a single neutral atom. Collision energy $E_{\mathrm{CM}} = 80$ eV. Prediction of the binary model as in Fig. 6.

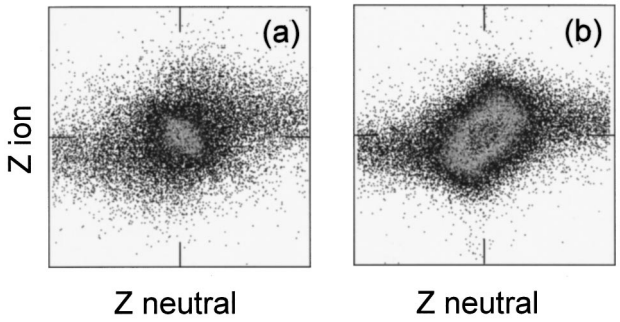

FIG. 10. Zooming on the bulky structures of the *ZZ* correlation patterns showing the dominance of the (a) EM mechanism for $Na_4^+ \rightarrow Na_2^+$ fragmentation at $E_{\mathrm{CM}} = 200$ eV and of (b) the IM2 mechanism $Na_5^+ \rightarrow Na_3^+$ at $E_{\mathrm{CM}} = 161$ eV.

not be explained by such IM1 alone. Actually this behavior is understood if one further assumes that, after the ejection of the fast Na atom, the hit cluster is left warm enough to evaporate additional Na or Na_2 fragments from the remaining Na_{n-1}^+ cluster depending on the endothermicity of the pathways. For example the contour lines of the $E_{\mathrm{rel}}(\chi)$ diagram of Fig. 9 drawn assuming such $Na_5^+ \rightarrow Na_3^+ + Na + Na$ two-step fragmentation pathway follow well the kinematics of an IM1 process at large E_{rel} and χ as in $Na_5^+ \rightarrow Na_4^+$. The strong peaking in the collision plane ($\Phi = 0$) of the $\Phi(\chi)$ distribution also favors this interpretation.

The bulky structure involves two contributions similarly to the release of a unique Na atom: (i) a two step (IM2) mechanism with a full redistribution of the momentum initially given by a binary He Na collision through multiple intracluster collisions [Fig. 10(b)]; (ii) an EM mechanism responsible for the backslash structure [Fig. 10(a)]. Both mechanisms may lead either to evaporation of two Na atoms or to a release of one Na_2 dimer. For each $Na_n^+ \rightarrow Na_{n-2}^+$ fragmentation pathway, the branching ratio $P_{\mathrm{Na+Na/Na_2}}$ (see Sec. III) irrespective to the fragmentation mechanism has been compared to the relative contribution of IM1. This comparison shows that the contribution of the release of two slow Na atoms is negligible with respect to that of one atom following the ejection of the fast Na (IM1). Such finding clearly shows a preferential adiabatic fragmentation of IM2 and EM processes along the less endothermic pathway[6,7] or, in other words, three particle $Na_n^+ \rightarrow Na_{n-2}^+ + Na + Na$ fragmentation is exclusively induced by an IM1 mechanism. The relative contributions of the various mechanisms for the $Na_n^+ \rightarrow Na_{n-1}^+$ and $Na_n^+ \rightarrow Na_{n-2}^+$ fragmentation pathway are given in Table I. This illustrates the key role of the electron pairing. For example, the ejection of a Na_2 dimer from an even and an odd cluster are induced by EM and IM2, respectively, as also illustrated by the shapes of the bulky structures for $Na_4^+ \rightarrow Na_2^+$ and $Na_5^+ \rightarrow Na_3^+$ fragmentation (Fig. 10). Another aspect of the electron pairing is the absence of IM2 contributions (small E_{rel}) to the $Na_n^+ \rightarrow Na_{n-1}^+$ channel for odd clusters [Fig. 6(a)], since the adiabatic behavior leads for soft collision to the production of Na_2.

IX. DISCUSSION AND CONCLUSION

In addition to fragmentation mechanisms presented above, *multiple collisions* between the target and several atomic cores of the cluster might play a significant role. They were suggested as possible fragmentation dynamics of rare gas clusters,[5] metal clusters[14] at threshold collision energies and of C_{60} (Ref. 34) at keV energies. We have also previously proposed this mechanism to explain our results.[35] We have then performed a simple molecular dynamics (MD) simulation, based on pairwise potentials, to investigate such dynamics in the Na_3^+ fragmentation.[36] Calculations show that such mechanism plays a minor role here, but its importance increases with the initial internal energy of the cluster and cannot be excluded for dissociation of larger clusters.

From the present analysis of the various fragmentation pathways, a first finding is that release of Na^+ fragments, at least for the smallest ($n = 3-5$) clusters, primarily involves electronic transitions towards dissociative states. In contrast, all other channels are populated via momentum transfer in binary collisions with a Na^+ core through one step and two step dynamics. This latter mechanism becomes dominant for large clusters (Table I) and shows up through two distinct mechanisms: either ejection of a fast fragment followed by the evaporation of slower ones (IM1) or a heating of the hit cluster via Na–Na collisions before evaporation of one or several fragments (IM2). Therefore fragmentation dynamics in the 100 eV CM collision energy range seems at variance with that operating at low eV energies where only evaporative mechanisms are generally invoked. However, as at low energy, populations of the various pathways are primarily governed by the relative endothermicities that, in turn, follow an odd even alternation reflecting the electron pairing. A simple model[30] based on a statistical distribution of the energy deposited by binary Na He elastic collisions reproduces the overall trends of the fragmentation probabilities (Fig. 2) but not the detailed behavior. The underestimated abundance of the odd ionic fragments might be explained by additional evaporations. The role of electron pairing in the fragmentation process was already pinpointed by Nonose *et al.*[6,7] in the preferential ''adiabatic'' release of a Na_2 dimer following Na_9^+ dissociation. Such behavior is also found here at higher collision energy. For example, pathways only populated via a direct ejection of a single fast Na fragment are not the rule and are found only when endothermicities are not favorable ($Na_5^+ \rightarrow Na_4^+$ and $Na_7^+ \rightarrow Na_6^+$). The pairing effect also shows up in the relative contribution of the electronic and impulsive

dynamics. EM shows up more distinctly with even clusters as it can be guessed from the orientation and shape of the bulky structures in the *ZZ* correlation patterns. However the overall contribution of the electronic mechanism to the total fragmentation never exceed 30% consistently with the estimation given by the TRIM compilation for stopping power.[37] One must finally stress that the initial temperature of the cluster should play a key role in the relative importance of the various mechanisms and hence in the branching ratios between the pathways.

[1] P. B. Armentrout, D. A. Hales, and Li Lian, *Advance in Metal and Semiconductor Clusters 2* (JAI, New York, 1994), pp. 1–39, and references therein.

[2] M. F. Jarrold and J. E. Bower, J. Phys. Chem. **92**, 5702 (1988); M. F. Jarrold, J. E. Bower, and J. S. Kraus, J. Chem. Phys. **86**, 3876 (1987); M. F. Jarrold and J. E. Bower, *ibid.* **85**, 5373 (1986).

[3] L. Hanley, S. A. Ruatta, and S. L. Anderson, J. Chem. Phys. **87**, 260 (1987).

[4] C. A. Woodward and A. J. Stace, J. Chem. Phys. **94**, 4234 (1991); A. J. Stace, P. G. Lethbridge, J. E. Upham, and C. A. Woodward, J. Chem. Soc., Faraday Trans. **86**, 2405 (1990); C. A. Woodward, J. E. Upham, and A. J. Stace, Chem. Phys. Lett. **158**, 417 (1989).

[5] J. Hirokawa, M. Ichihashi, S. Nonose, T. Tahara, T. Nagata, and T. Kondow, J. Chem. Phys. **101**, 6625 (1994).

[6] S. Nonose, H. Tanaka, T. Mizumo, J. Hirokawa, and T. Kondow, J. Chem. Phys. **104**, 5869 (1996).

[7] S. Nonose, H. Tanaka, T. Mizuno, N. J. Kim, K. Someda, and T. Kondow, J. Chem. Phys. **105**, 9167 (1996).

[8] F. Rohmund, E. E. B. Campbell, O. Knospe, G. Seifert, and R. Schmidt, Phys. Rev. Lett. **76**, 3289 (1996).

[9] B. Farizon, M. Farizon, M. J. Gaillard, E. Gerlic, S. Louc, N. V. de Castro Faria, and G. Jalbert, Chem. Phys. Lett. **252**, 147 (1996).

[10] B. Farizon, M. Farizon, M. J. Gaillard, F. Gobet, M. Carré, J. P. Buchet, P. Schier, and T. D. Märk, Phys. Rev. Lett. **81**, 4108 (1998).

[11] K. Wohrer, M. Chabot, J. P. Rozet, D. Gardès, D. Vernhet, D. Jacquet, S. Della Negra, A. Brunelle, M. Nectoux, M. Pautrat, and Y. Le Beyec, Phys. Scr. **T73**, 284 (1997).

[12] F. Chandezon, C. Guet, B. A. Huber, D. Jalabert, M. Maurel, E. Monnand, C. Ristori, and J. C. Rocco, Phys. Rev. Lett. **74**, 3784 (1995).

[13] P. de Sainte Claire, G. H. Peslherbe, and W. L. Hase, J. Phys. Chem. **99**, 8147 (1995).

[14] P. de Sainte Claire and W. L. Hase, J. Phys. Chem. **100**, 8190 (1996).

[15] U. Saalmann and R. Schmidt, Z. Phys. D **38**, 153 (1996); R. Ehlich, O. Knospe, and R. Schmidt, J. Phys. B **30**, 5429 (1997).

[16] D. Babikov, F. Aguillon, M. Sizun, and V. Sidis, Phys. Rev. A **59**, 330 (1999).

[17] M. Gross and C. Guet, Z. Phys. D **33**, 289 (1995); Phys. Rev. A **54**, R2547 (1996).

[18] J. Los and T. R. Govers, *Collision Spectroscopy*, edited by R. G. Cooks (Plenum, New York, 1978), p. 289; J. Durup, *Recents Developments in Mass Spectrometry*, edited by K. Ogata and T. Hayakwa (University of Tokyo Press, Tokyo, 1970), p. 921.

[19] J. Lindhard, Mat. Fys. Medd. K. Dan. Vidensk. Selsk. **28**, 1 (1954); J. Lindhard, and A. Whinter, *ibid.* **34**, 1 (1965).

[20] D. P. de Bruijn, J. Neuteboom, V. Sidis, and J. Los, Chem. Phys. **85**, 215 (1984); D. P. de Bruijn and V. Sidis, *ibid.* **85**, 201 (1984).

[21] B. H. Mahan, J. Chem. Phys. **52**, 5221 (1970).

[22] P. J. Robinson and K. A. Holbrook, *Unimolecular Reaction* (Wiley–Interscience, London, 1972).

[23] C. Bréchignac, Ph. Cahuzac, J. Leygnier, R. Pfaum, and J. Weiner, Phys. Rev. Lett. **61**, 314 (1988).

[24] J. C. Brenot, H. Dunet, J. A. Fayeton, M. Barat, and M. Winter, Phys. Rev. Lett. **77**, 1246 (1996).

[25] J. A. Fayeton, M. Barat, J. C. Brenot, H. Dunet, Y. J. Picard, R. Schmidt, and U. Saalmann, Phys. Rev. A **57**, 1058 (1998).

[26] M. Barat, J. C. Brenot, H. Dunet, J. A. Fayeton, and Y. J. Picard, Eur. Phys. J. D **1**, 271 (1998).

[27] M. Barat, J. C. Brenot, H. Dunet, J. A. Fayeton, Y. J. Picard, D. Babikov, and M. Sizun, Chem. Phys. Lett. (in press).

[28] Y. J. Picard, M. Barat, J. C. Brenot, H. Dunet, and J. A. Fayeton (to be published).

[29] B. Brehm, J. Grosser, T. Ruscheinski, and M. Zimmer, Meas. Sci. Technol. **6**, 953 (1995).

[30] M. Barat, J. C. Brenot, H. Dunet, and J. A. Fayeton, Z. Phys. D **40**, 323 (1997).

[31] Y. Wang, T. F. George, D. M. Lindsay, and A. C. Beri, J. Chem. Phys. **86**, 3493 (1987); D. M. Lindsay, Y. Wang, and T. F. George, *ibid.* **86**, 3500 (1987).

[32] C. Bréchignac, Ph. Cahuzac, J. Leygnier, and J. Weiner, J. Chem. Phys. **90**, 1492 (1989).

[33] P. C. Engelking, J. Chem. Phys. **87**, 936 (1987).

[34] M. C. Larsen, P. Hvelplund, M. O. Larsson, and Hao Shen, Eur. Phys. J. D **5**, 283 (1999).

[35] M. Barat, J. C. Brenot, H. Dunet, J. A. Fayeton, and Y. J. Picard, Comments At. Mol. Phys. **34**, 329 (1999).

[36] Y. J. Picard, thèse de doctorat de l'université Paris Sud, 1999 (unpublished).

[37] J. F. Ziegler and J. P. Biersack, *The Stopping and Range of Ions in Solids* (Pergamon, New York, 1985).